



Free electrons excited SPASER

Y. Ye^{1,2,3}, F. Liu,^{1,2,3,*} K. Cui^{1,2,3}, X. Feng^{1,2,3}, W. Zhang^{1,2,3}, AND Y. Huang^{1,2,3}

¹Department of Electronic Engineering, Tsinghua University, Beijing 100084, China

²Beijing National Research Center for Information Science and Technology, Beijing, China

³Beijing Academy of Quantum Information Science, Beijing, China

*liu_fang@tsinghua.edu.cn

Abstract: Surface plasmon amplification by stimulated emission of radiation (SPASER) is discovered and used for realizing lasers at nanometer scale. The conventional gain media that are applied in SPASER are solid materials, such as organic dye or semiconductor, which limits the frequency range of SPASER. The free electrons could be considered as a kind of gain medium for emitting radiation. Here, we investigate theoretically the SPASER, which is excited by free electrons. We also demonstrate the tunable, deep-ultraviolet, and ultracompact laser numerically by having free electrons interact with surface plasmon polariton mode supported on metal surface. The output power density could reach about $30 \text{ W}/\mu\text{m}^2$ and the wavelength in deep ultraviolet could be widely tuned by varying the electron energy. This work offers a way of realizing integrated free electron laser in the ultraviolet frequency region.

© 2018 Optical Society of America under the terms of the [OSA Open Access Publishing Agreement](#)

1. Introduction

Surface plasmon polariton (SPP) is the resonant oscillation between electrons on metal surface and electromagnetic (EM) wave [1,2]. For the special characteristics, it attracts great attention in recent years for the potential applications of sensing [3–5], integrated optical circuit [6,7], and nanoscale laser [8–10]. By introducing gain medium adjacent to metal, the surface plasmon amplification by stimulated emission of radiation (SPASER) was discovered and used for realizing lasers at nanometer scale with remarkable advantages [8–16]. However, the previous plasmonic lasers were based on gain medium like organic dye or semiconductor which emits SPP mainly in near-infrared and visible frequency region [8–10,12–15]. Restricted by the gain medium, it seems hard to greatly shorten the vacuum wavelength of SPASER to deep ultraviolet and tune the wavelength in a wide range.

Free electrons flying in free space or media could be considered as a super broadband evanescent light source [17] and generate EM radiation such as Cherenkov radiation [18–20] and Smith-Purcell radiation [21]. Having free electrons fly around metal structure, the plasmonic mode could be excited and the dispersion relation of SPP [22], the damping of localized surface plasmon mode [23], and the plasmonic nano-cavity properties [24] have been studied. Recently, the surface polariton Cherenkov source [25] and Smith-Purcell radiation in plasmonic crystals [26] provide new ways for free electron light sources. In these previous works, the plasmonic mode has no feedback on the free electrons and no stimulated effect could happen. While in the process of stimulated Cherenkov radiation [27] and Smith-Purcell radiation [28], the radiation generated by free electrons results in bunching of free electrons and then the stimulated emission occurs. Based on stimulated Cherenkov radiation and Smith-Purcell radiation, the free electron laser could be realized [27–32].

In this paper, inspired by the SPASER [11] and the stimulated Cherenkov radiation with free electrons modulated by EM radiation [27,29–32], we propose a SPASER with the free electrons as gain medium based on the stimulated effect between free electrons and plasmonic mode. We investigate theoretically the free electrons excited SPASER and demonstrate numerically the tunable, deep-ultraviolet, ultracompact laser by having free electrons interact

with surface plasmon polariton mode supported on metal surface. The gain of SPP induced by free electrons is calculated and the numerical simulation shows that the stimulated amplification of SPP at center wavelength of 126 nm with linewidth of 0.3 nm and output power density of $30 \text{ W}/\mu\text{m}^2$ could be generated. Furthermore, the wavelength could be tuned from visible to deep UV via modifying the kinetic energy of free electrons and using different metal.

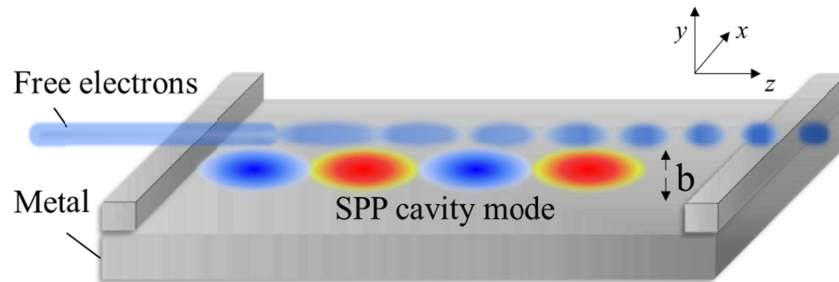


Fig. 1. Schematic of free electrons excited SPASER. Electron beam flies above Al film along z direction with gap b . Two Al mirrors are located at the two ends of metal slab to form SPP cavity. The interaction of SPP mode in cavity and free electrons results in the stimulated emission of SPP.

Figure 1 illustrates the schematic of free electrons excited SPASER. Having free electron beam fly on metal surface, the SPP mode could be excited. Two Al mirrors are located at the two ends of the metal slab to form SPP cavity and the continuous electron-SPP interaction results in the bunching of electron beam and stimulated emission of SPP. Parts of the SPP would be scattered into free space at the end of metal slab and detected. Different from nanoscale SPP cavity [24], here the cavity length is much larger than SPP wavelength to ensure the SPP has sufficient interaction and feedback on free electrons.

The physical mechanism of free electrons excited SPASER can be understood as follows. The super broadband evanescent wave surrounding free electrons would excite the SPP mode around the frequency of phase-matching point (in a frequency range) [25]. The SPP mode would bunch the free electron beam (speed up/slow down part of the free electrons), and the SPP modes with phase velocity slightly slower than that of free electrons will decelerate electrons and get energy (namely the gain compensation) from them. Furthermore, the cavity enables continuous interaction between SPP and free electrons, which results in the stronger bunching of free electron beam. The bunched electron beam will produce radiation field that superimposes in phase and generate strong stimulated emission of radiation [28–30] to form positive feedback, making it possible to obtain laser oscillation and high-power radiation. This process is similar to stimulated Cherenkov radiation [27], but here the SPP mode is excited and amplified rather than photon. Thus, this phenomenon is referred as free electron excited SPASER in this paper. Compared with stimulated Cherenkov radiation, it has three advantages: (1) the enhanced field of SPP mode could greatly enhance the stimulated effect; (2) the SPP mode could greatly reduce the device to nanoscale dimensions; (3) the frequency of radiation could be much higher (in deep UV region) by selecting metal material. Compared with SPASER using solid gain materials, the frequency of free electrons excited SPASER is not limited by the gain materials and could also be tuned easily.

2. Theoretical study of the frequency and gain of SPASER

In this section, a simplified two-dimensional (2D) model is applied for theoretical analysis. The frequency of SPP mode excited by free electrons and the mode spatial growth rate α are calculated theoretically, which provides an estimation of current density needed for SPASER in simulation. The model is shown in Fig. 2(a), a semi-infinite metal and an electron beam moving with constant velocity (v_0) along z direction is separated by a narrow vacuum gap (b).

The calculation region is divided into three regions: region I is vacuum including a sheet electron beam with plasma frequency ω_p and velocity v_0 along z direction, region II is vacuum and region III is a semi-infinite metal.

Figure 2(b) shows the dispersion curve of SPP (orange) on metal surface and evanescent wave around electron beam (violet) with velocity of v_0 (corresponding kinetic energy E_0). For electron beam with low electron density, if the plasma frequency ω_p is much lower than frequency ω ($\omega_p \ll \omega$), the dispersion relation of the evanescent wave around electron beam could be written as $\omega = v_0 k$ [17], where k is the wave number in z direction. For SPP on metal surface, its dispersion relation is $k_{SPP} = (\omega/c)\sqrt{\epsilon_m/(\epsilon_m+1)}$ [1,2], where ϵ_m denotes the relative permittivity of metal. The intersection of violet and orange line (red point k_{z0}) in Fig. 2(b) indicates the phase velocity matching frequency, around which strong mode coupling will occur and SPASER could be obtained.

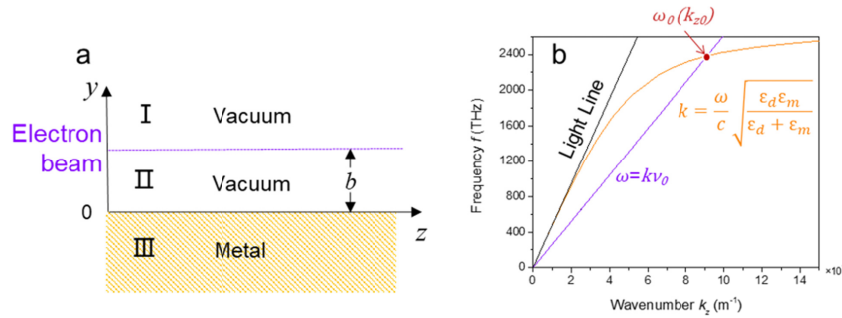


Fig. 2. (a) The two-dimensional model for calculating the mode coupling between evanescent wave around free electron and SPP on metal surface. An electron beam (purple dot line) and a semi-infinite metal are separated by a vacuum gap. (b) Dispersion relation of SPP on metal film (orange curve) and evanescent wave around electron beam (violet line). Around the red intersect point k_{z0} , the SPP is excited by free electrons.

The growth rate α could be derived from the dispersion relation of the coupling mode between SPP mode and evanescent wave around free electrons. According to Maxwell equation with free electrons of plasma frequency ω_p and velocity v_0 along z direction and dispersion relation of SPP, the field components of EM wave in the three regions of the 2D model have been well-established in previous works [1,27]. And combined with the boundary conditions, the dispersion relation of the coupling mode could be derived as:

$$\epsilon_p \left(\frac{p_y}{k_y} + \frac{\epsilon_m h_y}{k_y} \tanh h_y b \right) + \frac{p_y}{h_y} \tanh h_y b + \epsilon_m = 0, \quad (1)$$

where $\epsilon_p = 1 - \omega_p^2 / \gamma^2 (\omega - v_0 k_z)^2$, $\gamma = 1 / \sqrt{1 - (v_0/c)^2}$ is the Lorentz factor, c is the light velocity in vacuum, k_z is the wave number along z direction, $k_y = \sqrt{k_z^2 - (\omega/c)^2 - (\omega_p/c)^2}$ is the wave number along y direction in region I, $h_y = \sqrt{k_z^2 - (\omega/c)^2}$ is the wave number along y direction in region II, and $p_y = \sqrt{k_z^2 - \epsilon_m (\omega/c)^2}$ is the wave number along $-y$ direction in region III.

In the vicinity of intersection shown in Fig. 2(b), we have $p_y / h_y + \epsilon_m \approx 0$ and $h_y \approx k_y$ for low density electron beam with $\omega_p \ll \omega$ (assuming $\omega_p = 0.01\omega$ in calculation). Therefore, Eq. (1) could be simplified to:

$$-e^{2h_y b} \left(\epsilon_m + \frac{p_y}{h_y} \right) (\omega - v_0 k_z)^2 = \epsilon_m \frac{\omega_p^2}{\gamma^2}. \quad (2)$$

Then we keep $\omega = \omega_0$ and seek solution for k_z . Around the intersection point, k_z could be expressed as $k_z = k_{z0} + \delta k$ and $\delta k \ll k_{z0}$ is assumed. From Eq. (2), we have

$$\delta k = \left[2\epsilon_m \left(\frac{\omega_p}{\gamma v_0} \right)^2 \frac{e^{-2h_y b}}{\frac{\partial}{\partial k_z} \left| \frac{p_y}{h_y} \right|} \right]^{\frac{1}{3}} e^{j \frac{2n\pi}{3}} \quad (n = 0, 1, 2), \quad (3)$$

where $h_{y0} = \sqrt{k_{z0}^2 - (\omega_0/c)^2}$, and the differentiation with respect to k_z is carried out at $k_z = k_{z0}$. For $n = 1$, the negative imaginary part of δk is defined as spatial growth rate α , which indicates that a growing SPP wave is excited by the electron beam. The spatial growth rate α could be derived as:

$$\alpha = \text{Im}(\delta k) = \frac{\sqrt{3}}{2} \left[2\epsilon_m \left(\frac{\omega_p}{\gamma v_0} \right)^2 \frac{e^{-2h_y b}}{\frac{\partial}{\partial k_z} \left| \frac{p_y}{h_y} \right|} \right]^{\frac{1}{3}}. \quad (4)$$

Because propagation loss of SPP α_{loss} (the imaginary part of k_{SPP}) cannot be ignored here, we define the net spatial growth rate as $g = \alpha - \alpha_{loss}$.

Assuming the electron-metal gap is $b = 50$ nm and the metal is Al with negative permittivity ϵ_m in UV region [33], Fig. 3 shows the calculated result of net spatial growth rate g according to Eq. (4) for different frequency and current density of electron beam. It can be seen that g increases with the current density of electron beam from 10^5 A/ μm to 10^7 A/ μm . With the same plasma frequency of electron beam, the corresponding current densities in the three-dimension (3D) model for simulation in the next section could be calculated [34] and presented in the parentheses. The positive net spatial growth rate g in UV guarantees that initially weak SPP will eventually lead to powerful output intensity. When current density is below 10^5 A/ μm (0.1 A/ μm^2), the SPP mode can hardly get positive g due to the propagation loss. As discussed in Fig. 2(b), for different electron energy E_0 (velocity v_0), the frequency ω of excited SPP is different shown as inset in Fig. 3. The corresponding gain α of SPP is mainly decided by the photonic density of state of SPP mode [20,35], which increases as frequency close to the surface plasmon resonant frequency (ω_{SP}) around 2400THz. Meanwhile the propagation loss increases rapidly at high frequency over 2300 THz (excited by electron with $E_0 < 130$ keV) leading to the sharp decrease of g with E_0 as shown in Fig. 3.

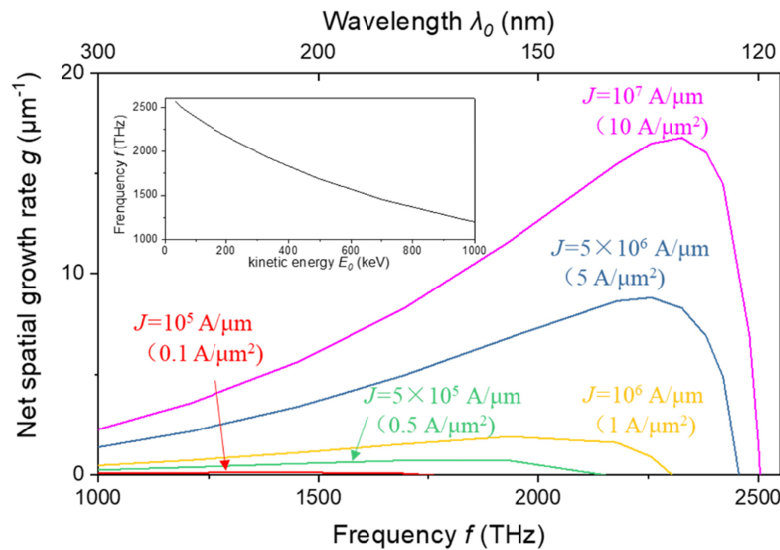


Fig. 3. Net spatial growth rate g for different frequency (top horizontal axis is wavelength) and current density of 10^7 A/ μm (magenta), 5×10^6 A/ μm (blue), 10^6 A/ μm (yellow), 5×10^5 A/ μm (green) and 10^5 A/ μm (red), the corresponding current densities for 3D model used in simulation are presented in parentheses. The inset shows frequency of SPP mode excited by electron beam with kinetic energy of electron E_0 . Here, the gap $b = 50$ nm and the metal is selected as Al.

The SPP frequency excited by electron beam and current density for SPASER (namely positive net spatial growth rate) are derived according to the theoretical calculation above. In the next section, the simulation will verify the SPASER excited by free electrons and show more details about the process including electron bunching and the evolution of output spectra and power. According to the calculation result that the higher current density, the higher net gain. And limited by the computer capacity, a much higher current of electron beam is set to obtain SPASER more quickly and save computing resources in the simulation.

3. Simulation of free electron excited SPASER

To simulate the process of SPASER excited by free electrons, the finite different time domain-particle in cell (FDTD-PIC) numerical algorithm is utilized with commercial software CST [36]. By self-consistently solving the coupled Maxwell and Newton-Lorentz equations [32], the EM distribution and particle state are calculated.

The 3D simulation model is shown in Fig. 1. The kinetic energy of electron beam is set as 100 keV with beam radius of 20 nm. In order to reduce the simulation time, the current of electron beam is assumed as 1 A. The relative high current would provide a higher net spatial growth rate and shorten the simulation time. The length (z direction), width (x direction), and thickness (y direction) of the Al layer are 1 μm , 500 nm, and 100 nm, respectively. The gap between the metal surface and electron beam is $b = 50$ nm. The Al mirrors are 30 nm high. A probe outside the SPP cavity (100 nm away from the right side SPP mirror) is set to monitor the output spectra and intensity of SPASER. The frequency of free electrons excited SPASER is decided by both SPP cavity length and free electrons (gain material). Since the cavity length is about 15 times larger than SPP wavelength and the free spectral range of SPP cavity modes is rather small (about 2 nm), the SPP frequency excited in cavity is in the vicinity of intersection of two curves in Fig. 2(b) and mainly decided by the velocity of electron.

Figure 4 shows the output spectra at the probe and EM distribution (E_z component) as electron beam with kinetic energy $E_0 = 100$ keV flies above Al film at different moment t . It is illustrated that the SPP at metal-vacuum interface is excited with field confined at metal-

vacuum interface and decaying rapidly as distance away from the interface. When $t = 200$ fs, Fig. 4(a) illustrates the output spectrum and EM distribution of SPP standing wave at different frequencies. The output spectrum peaks at 2381 THz ($\lambda_0 = 126$ nm) and has relatively low intensity at frequencies of 2376 THz and 2402 THz. The relatively broadband spectrum indicates that the SPP mode has been excited around phase velocity matching frequency and the stimulated radiation has not occurred yet. When $t = 2900$ fs, the spectrum and EM field distribution in Fig. 4(b) illustrate that the SPP mode has much stronger intensity (four orders of magnitude higher) and narrower spectrum width (full width at half maximum ~ 2 THz) than that at $t = 200$ fs (~ 15 THz), which indicates that the generation of SPASER.

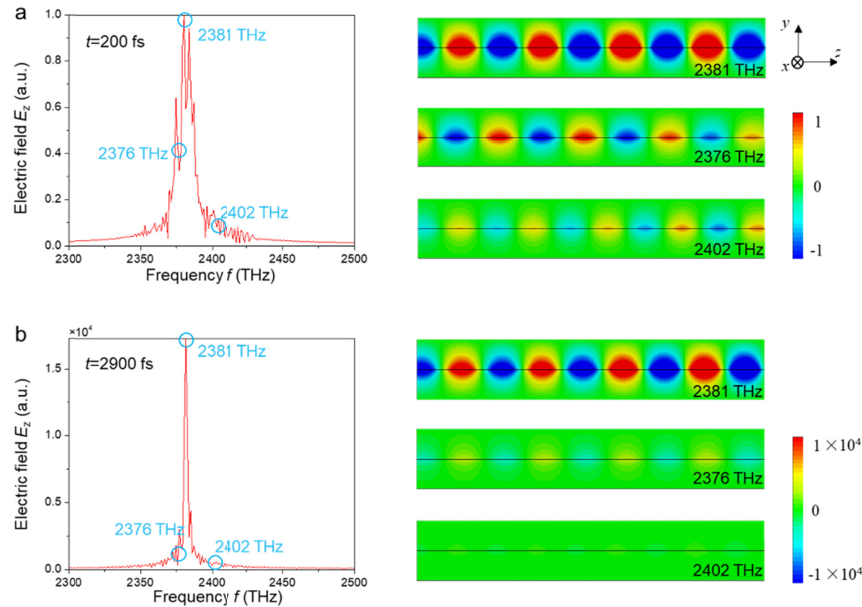


Fig. 4. The output spectra and EM distribution of SPP standing waves at (a) $t = 200$ fs and (b) $t = 2900$ fs. The spectrum width at $t = 200$ fs is much narrower than that at $t = 200$ fs and the intensity of SPP is more than four orders of magnitude higher. With stimulated effect, (main component of electric field, E_z). The SPP mode is excited by electron beam of 100 keV and 1A. The EM field and output spectra in (a) and (b) are normalized to the corresponding maximum value at $t = 200$ fs.

Analogous to stimulated Cherenkov radiation, another important feature revealed by the free electrons excited SPASER is the bunching of electron beam due to the interaction between electrons and EM field [27,32]. Figure 5 shows the simulation results of spatial electron density at different moment t . At $t = 200$ fs illustrated in Fig. 5(a), the electron density is almost uniform along z direction, namely the electrons have almost the same velocity. The SPP mode has been excited by electron beam, but its intensity is too weak to greatly affect the electrons. The SPP could be considered as spontaneous radiation with relative wide spectrum shown in Fig. 4(a). At $t = 2900$ fs shown in Fig. 5(b), the electron density has obvious spatial periodic distribution of ~ 68 nm, which is close to the SPP wavelength. This is because the intensity of SPP increases for continuous electron beam excitation and the strong SPP field bunches the electron beam (accelerate/decelerate some of the electrons) with a period of SPP wavelength. The bunched electron beam further produce radiation field that superimposes in phase and the SPP intensity would be greatly increased. The positive feedback results in the SPASER with spectrum shown in Fig. 4(b).

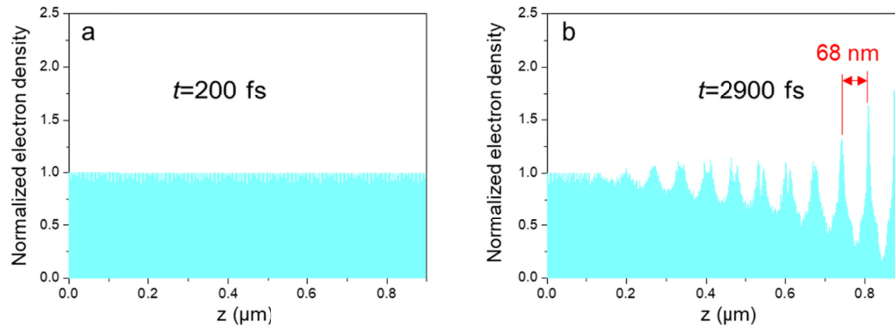


Fig. 5. The distribution of electron density along z direction at (a) $t = 200$ fs and (b) $t = 2900$ fs. The electron density is normalized to its value at $z = 0$.

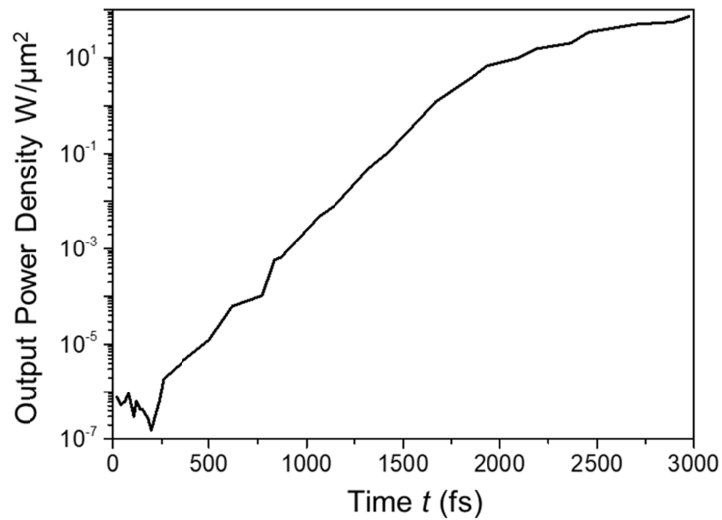


Fig. 6. The evolution of output power of SPASER. The output power increases exponentially (250 fs-2500 fs) for the stimulated effect and is saturated at a power density around $30 \text{ W}/\mu\text{m}^2$ after $t = 2500$ fs.

The optical amplification process is also revealed by the evolution of SPP intensity as shown in Fig. 6. Initially, the output power detected by probe is weak (about 1 nW) and the power density is of $10^{-7} \text{ W}/\mu\text{m}^2$. Then the output power begins to grow exponentially indicating a signature of stimulated effect. After 2900 fs, the power growth begins to slow down and saturate to about $30 \text{ W}/\mu\text{m}^2$, which is over eight orders of magnitude higher than initial value. The evolution of output spectra in Fig. 4, the bunching of free electrons in Fig. 5 and the evolution of output power indicate the SPASER in deep UV ($\lambda_0 = 126 \text{ nm}$) has been generated.

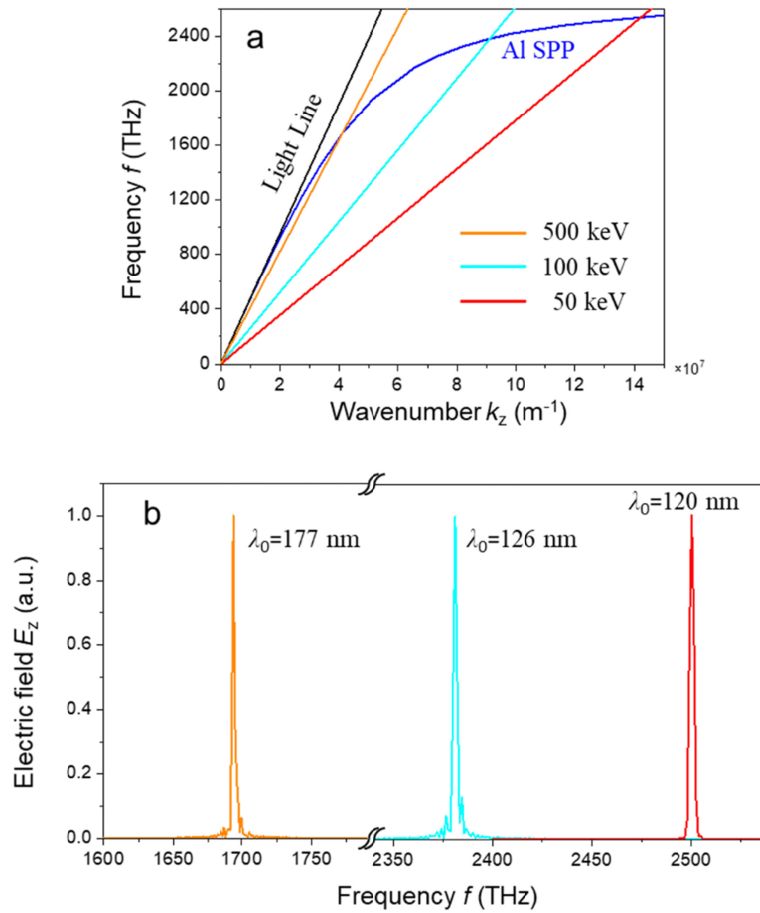


Fig. 7. (a) Dispersion relation of SPP on Al (blue) surface and evanescent wave surrounding electron beam with energy of 500 keV (orange), 100 keV (cyan), 50 keV (red). (b) The simulation results of spectra of SPASER on Al surface generated by electron beam with energy of 500 keV (orange), 100keV (cyan) 50 keV (red) electron beam. The corresponding center wavelengths of SPASER are $\lambda_0 = 177$ nm, 126 nm, 120 nm, respectively, and the 3 dB spectrum width is less than 0.5 nm.

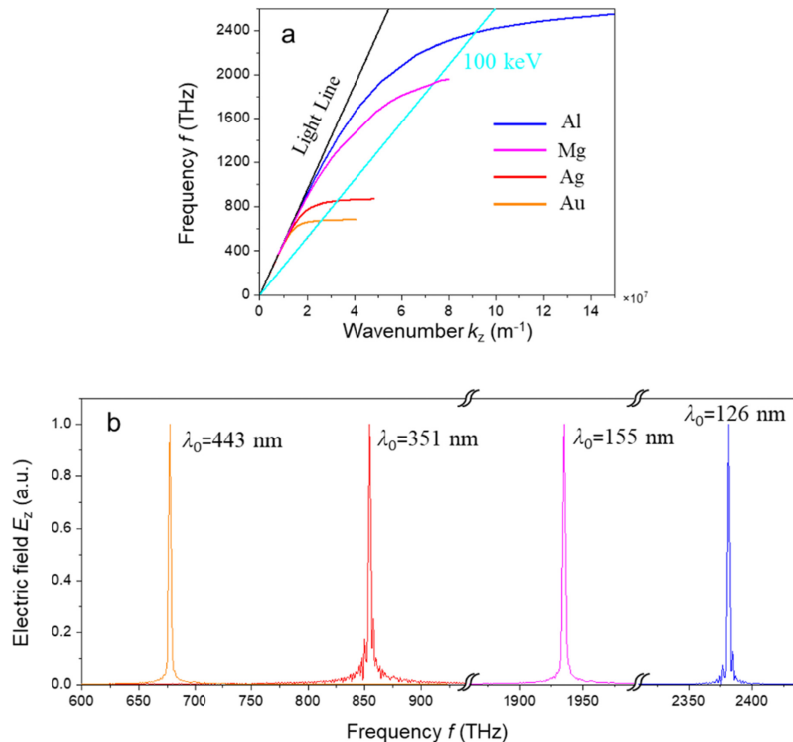


Fig. 8. (a) Dispersion relation of SPP on Al (blue), Mg (magenta), Ag (red), Au (orange) surface and evanescent wave surrounding electron beam with energy of 100 keV (cyan). (b) The output spectra of SPASER on Al (blue), Mg (magenta), Ag (red), Au (orange) surface generated by electron beam with energy of 100 keV (red). The center wavelengths of SPASER are $\lambda_0 = 126$ nm, 155 nm, 351 nm, 443 nm respectively.

The wavelength of SPASER could be tuned by modifying kinetic energy of electron beam. Figure 7(a) shows the frequencies of SPASER (intersections of blue curve with orange, cyan and red line) increase as kinetic energy of electron beam decreases. The simulated spectra of SPASER are shown in Fig. 7(b) with frequency in good agreement with the intersections in Fig. 7(a). It is indicated that, by adjusting the electron energy from 50 keV to 500 keV, the SPASER could be tuned in a wide range from 120 nm to 177 nm in the deep UV region. By applying different metal material with different permittivity, the SPASER could be generated in a wider frequency range from visible to deep UV. As plotted in Fig. 8(a), the cyan line of 100keV electron beam interacts with SPP curve supported by Au, Ag, Mg and Al, respectively. And the SPASER could be obtained in visible ($\lambda_0 \approx 443$ nm), near UV ($\lambda_0 \approx 351$ nm), and deep UV ($\lambda_0 \approx 155$ nm, 126 nm) region, which is also demonstrated by the simulated spectra in Fig. 8(b). Thus, by adjusting the electron energy and selecting metal material, the SPASER could be derived from visible to deep UV.

4. Conclusion

In this paper, we study the SPASER excited via free electrons by having electron beam interact with SPP mode on metal surface and the SPASER could be obtained in deep UV region. The gain of SPP mode with different frequency excited by free electron with different velocity is calculated theoretically, which indicates a current density of 10^5 A/ μm for 2D model (0.1 A/ μm^2 for 3D model) is needed to overcome the propagation loss and obtain net spatial growth rate. The simulation results verify the SPASER by observing the evolution of

electron beam bunching, output power and spectrum width. It is demonstrated numerically that, for electron beam of 100keV and 1A flying on Al surface, the SPASER with wavelength of $\lambda_0 = 126$ nm, spectrum width (FWHM) less than 2 THz (center frequency 2381 THz, FWHM 0.3 nm) and power density over $30 \text{ W}/\mu\text{m}^2$ is obtained. Besides, the output wavelength could be tuned from 120 nm to 177 nm by modifying kinetic energy of electron beam from 50~500keV. While using other metal, the output wavelength of SPASER could be altered in a wider range (from UV to visible). The free electrons excited SPASER provides a way for realizing tunable and ultracompact laser in deep UV region.

Funding

National Basic Research Programs of China (973 Program) under Contracts No. 2013CBA01704; the National Natural Science Foundation of China (NSFC-61575104 and 61621064); Beijing Innovation Center for Future Chip and Beijing Academy of Quantum Information Science.

References

1. W. L. Barnes, A. Dereux, and T. W. Ebbesen, "Surface plasmon subwavelength optics," *Nature* **424**(6950), 824–830 (2003).
2. S. A. Maier and H. A. Atwater, "Plasmonics: Localization and guiding of electromagnetic energy in metal/dielectric structures," *J. Appl. Phys.* **98**(1), 011101 (2005).
3. B. Fan, F. Liu, X. Wang, Y. Li, K. Cui, X. Feng, and Y. Huang, "Integrated sensor for ultra-thin layer sensing based on hybrid coupler with short-range surface plasmon polariton and dielectric waveguide," *Appl. Phys. Lett.* **102**(6), 061109 (2013).
4. A. V. Kabashin, P. Evans, S. Pastkovsky, W. Hendren, G. A. Wurtz, R. Atkinson, R. Pollard, V. A. Podolskiy, and A. V. Zayats, "Plasmonic nanorod metamaterials for biosensing," *Nat. Mater.* **8**(11), 867–871 (2009).
5. O. Salihoglu, S. Balci, and C. Kocabas, "Plasmon-polaritons on graphene-metal surface and their use in biosensors," *Appl. Phys. Lett.* **100**(21), 213110 (2012).
6. R. F. Oulton, V. J. Sorger, D. A. Genov, D. F. P. Pile, and X. Zhang, "A hybrid plasmonic waveguide for subwavelength confinement and long-range propagation," *Nat. Photonics* **2**(8), 496–500 (2008).
7. F. Liu, Y. Rao, Y. Huang, W. Zhang, and J. Peng, "Coupling between long range surface plasmon polariton mode and dielectric waveguide mode," *Appl. Phys. Lett.* **90**(14), 141101 (2007).
8. R. F. Oulton, V. J. Sorger, T. Zentgraf, R. M. Ma, C. Gladden, L. Dai, G. Bartal, and X. Zhang, "Plasmon lasers at deep subwavelength scale," *Nature* **461**(7264), 629–632 (2009).
9. M. A. Noginov, G. Zhu, A. M. Belgrave, R. Bakker, V. M. Shalaev, E. E. Narimanov, S. Stout, E. Herz, T. Suteewong, and U. Wiesner, "Demonstration of a spaser-based nanolaser," *Nature* **460**(7259), 1110–1112 (2009).
10. R. M. Ma, S. Ota, Y. Li, S. Yang, and X. Zhang, "Explosives detection in a lasing plasmon nanocavity," *Nat. Nanotechnol.* **9**(8), 600–604 (2014).
11. D. J. Bergman and M. I. Stockman, "Surface plasmon amplification by stimulated emission of radiation: quantum generation of coherent surface plasmons in nanosystems," *Phys. Rev. Lett.* **90**(2), 027402 (2003).
12. N. I. Zheludev, S. L. Prosvirnin, N. Papasimakis, and V. A. Fedotov, "Lasing spaser," *Nat. Photonics* **2**(6), 351–354 (2008).
13. R. A. Flynn, C. S. Kim, I. Vurgaftman, M. Kim, J. R. Meyer, A. J. Mäkinen, K. Bussmann, L. Cheng, F.-S. Choa, and J. P. Long, "A room-temperature semiconductor spaser operating near $1.5 \mu\text{m}$," *Opt. Express* **19**(9), 8954–8961 (2011).
14. J. B. Khurgin and G. Sun, "Comparative analysis of spasers, vertical-cavity surface-emitting lasers and surface-plasmon-emitting diodes," *Nat. Photonics* **8**(6), 468–473 (2014).
15. D. Li and M. I. Stockman, "Electric spaser in the extreme quantum limit," *Phys. Rev. Lett.* **110**(10), 106803 (2013).
16. Q. Zhang, G. Li, X. Liu, F. Qian, Y. Li, T. C. Sum, C. M. Lieber, and Q. Xiong, "A room temperature low-threshold ultraviolet plasmonic nanolaser," *Nat. Commun.* **5**(1), 4953 (2014).
17. F. J. García de Abajo, "Optical excitations in electron microscopy," *Rev. Mod. Phys.* **82**(1), 209–275 (2010).
18. P. A. Čerenkov, "Visible radiation produced by electrons moving in a medium with velocities exceeding that of light," *Phys. Rev.* **52**(4), 378–379 (1937).
19. I. Frank and I. Tamm, *Coherent visible radiation of fast electrons passing through matter* (Springer, 1991).
20. F. Liu, L. Xiao, Y. Ye, M. Wang, K. Cui, X. Feng, W. Zhang, and Y. Huang, "Integrated Cherenkov radiation emitter eliminating the electron velocity threshold," *Nat. Photonics* **11**(5), 289–292 (2017).
21. S. J. Smith and E. M. Purcell, "Visible light from localized surface charges moving across a grating," *Phys. Rev.* **92**(4), 1069 (1953).
22. R. B. Pettit, J. Silcox, and R. Vincent, "Measurement of surface-plasmon dispersion in oxidized aluminum films," *Phys. Rev. B* **11**(8), 3116–3123 (1975).

23. P. E. Batson, "Damping of bulk plasmons in small aluminum spheres," *Solid State Commun.* **34**(6), 477–480 (1980).
24. X. L. Zhu, Y. Ma, J. S. Zhang, J. Xu, X. F. Wu, Y. Zhang, X. B. Han, Q. Fu, Z. M. Liao, L. Chen, and D. P. Yu, "Confined three-dimensional plasmon modes inside a ring-shaped nanocavity on a silver film imaged by cathodoluminescence microscopy," *Phys. Rev. Lett.* **105**(12), 127402 (2010).
25. S. Liu, P. Zhang, W. Liu, S. Gong, R. Zhong, Y. Zhang, and M. Hu, "Surface polariton Cherenkov light radiation source," *Phys. Rev. Lett.* **109**(15), 153902 (2012).
26. I. Kaminer, S. E. Kooi, R. Shiloh, B. Zhen, Y. Shen, J. J. López, R. Remez, S. A. Skirlo, Y. Yang, J. D. Joannopoulos, A. Arie, and M. Soljačić, "Spectrally and spatially resolved Smith-Purcell radiation in plasmonic crystals with short-range disorder," *Phys. Rev. X* **7**(1), 011003 (2017).
27. T. Shiozawa, *Classical Relativistic Electrodynamics* (Springer, 2004).
28. D. Li, Y. Wang, M. Nakajima, M. Tani, M. Hashida, M. R. Asakawa, Y. Wei, and S. Miyamoto, "Coherent radiation at the fundamental frequency by a Smith-Purcell free-electron laser with dielectric substrate," *Appl. Phys. Lett.* **110**(15), 151108 (2017).
29. E. Fisch, A. K. Henning, and J. Walsh, "A Cherenkov microlaser," *IEEE J. Quantum Electron.* **27**(3), 753–759 (1991).
30. E. P. Garate, S. Moustazis, J. M. Buzzi, C. Rouille, H. Lamain, J. Walsh, and B. Johnson, "Cherenkov maser operation at 1–2 mm wavelengths," *Appl. Phys. Lett.* **48**(20), 1326–1328 (1986).
31. Y. Wang, Y. Wei, D. Li, K. Takano, M. Nakajima, X. Jiang, X. Tang, X. Shi, Y. Gong, J. Feng, and S. Miyamoto, "Dispersion, spatial growth rate, and start current of a Cherenkov free-electron laser with negative-index material," *Phys. Plasmas* **22**(8), 083111 (2015).
32. T. Denis, M. W. van Dijk, J. H. H. Lee, R. van der Meer, A. Strooisma, P. J. M. van der Slot, W. L. Vos, and K.-J. Boller, "Coherent Cherenkov radiation and laser oscillation in a photonic crystal," *Phys. Rev. A (Coll. Park)* **94**(5), 053852 (2016).
33. E. D. Palik, *Handbook of Optical Constants of Solids* (Academic, 1985).
34. J. T. Donohue and J. Gardelle, "Simulation of Smith-Purcell radiation using a particle-in-cell code," *Phys. Rev. Spec. Top. Accel. Beams* **8**(6), 060702 (2005).
35. K. Joulain, R. Carminati, J.-P. Mulet, and J.-J. Greffet, "Definition and measurement of the local density of electromagnetic states close to an interface," *Phys. Rev. B Condens. Matter Mater. Phys.* **68**(24), 245405 (2003).
36. CST-computer simulation technology, <https://www.cst.com>.